Design of Ultrathin Metasurface for Multiview 3D Display Based on Look-Up-Table Method

Munzza Ahmad, Jingnan Li, Ruyi Zhou, Yutong Sun, and Juan Liu

***Abstract*—Multiview display has attention owing to its smooth motion parallax, visual discomfort alleviation, and wide depth of focus. Nevertheless, its applications are limited because of the freedom to design ultrathin display systems. This paper proposes a novel method to design the system freely by using ultrathin metasurface in conjunction with a flat panel to reduce the system's complexity. We demonstrate ultrathin metasurface for red (637 nm), green (532 nm), and blue (457 nm) wavelengths by using the look-up table method, and the subpixel of the metasurface are mapped according to the pixel arrangements of the LCD panel. The proposed 3D multiview display system produces 8 views at the optimal distance of 1000 mm from the LCD screen. Numerical simulation is implemented to verify the effectiveness of proposed method and the results show that it can achieve a multiview 3D display with high quality. The thickness of metasurface is 2 μm. The proposed metasurface for multiview display has great potential to underpin the development meta-optics-based operations in the field of integrated optics and imaging**

***Index Terms*—Multiview display, ultrathin metasurface, LCD panel, 3D displays, look-up table.**

I. Introduction

THREE-DIMENSIONAL display technologies incorporate volumetric 3D display [1], [2], [3], Maxwellian-view display [4], holographic display [5], light field display which comprise integral imaging [6], [7], tabletop display [8] and multi view display [9], [10], [11], [12]. However, multiview displays usually employ 2D displays and some associated optical devices to direct multiview images to multiple distinct viewing regions to implement both motion parallax and binocular parallax for the viewers. In conventional displays lenticular lenses and parallax barriers are used in front of flat display panels to redirect subpixels to different views. Lenticular lens employed in literature also suffers from aberrations and high cross talk to deteriorate the quality of the display. Furthermore, higher crosstalk results from aberrations of refraction-based optical components such as lenticular lenses [13]. Both lenticular lens and parallax barriers reduce the resolution by a factor of the number of views. The lower angular resolution also produces poor depth of field (DOF) [14], [15]. Researchers have done many works in the multiview display. Several techniques have been presented in the literature to overcome these drawbacks mentioned above. However, the use of lenticular lens array in conventional multiview displays makes the system complex and bulky.

Metasurface provide an effective light manipulation method for 3D displays to address the aforementioned critical issues, while making the system ultrathin compared to lenticular lens. Metasurfaces, are ultrathin structures which can manipulate the phase, amplitude and polarization of light at the subwavelength scale [16], [17], [18], [19], it can have strong potential for being easily integrated into on-chip optoelectronic systems in optical and microwave frequency regimes. Such a planar strategy can serve as a promising route for real-world applications [20], [21], [22]. The metasurface can imprint abrupt phase changes on each pixel to produce arbitrary phase distributions on propagating light through the delicate design of antennas. The significant benefits of the metasurface over traditional components of optical systems are great flexibility and ultrathin size [23], [24], [25]. They can also be designed for deflecting light [26], generating holograms [27], focusing [28], circular dichroism [29], [30], vortex beams production [31], modulating light intensity [32], lensing, imaging and beam splitting [33]. It can also be utilized to replace bulk optics for 3D imaging, in addition to conventional 2D imaging [34]. The advantage of their large numerical aperture and compact size make them useful in some innovative applications of beam shaping, holographic display and optical computing, which surpass the performance of diffractive optical elements and conventional lenses [35], [36]. Moreover, metasurfaces also revealed superiority in dispersion control, and many efforts have been made in broadband achromatic, multiwavelength control and enhanced chromatic dispersion [37]. They can eliminate chromatic aberration and provide image correction in imaging applications. The subwavelength pitch pixels of metasurface for 3D imaging systems can improve the diffraction efficiencies and field of view (FOV) by modulating the phase [38].

However, to the author knowledge, no study focuses to use metasurface for multiview 3D display. In the present study, we have proposed a multiview display system by using ultrathin metasurface. The look-up table (LUT) method is used in our design to map the metasurface phase for RGB wavelengths with the discrete phase distribution of lenticular lens array to obtain the metasurface array distribution for multiview display. 8 viewpoints are generated to satisfy the multiview condition,

Manuscript received 20 November 2023; revised 28 December 2023; accepted 9 January 2024. Date of publication 15 January 2024; date of current version 29 March 2024. This work was supported in part by the National key R&D program of China under Grant 2021YFB3600500, in part by the National Natural Science Foundation of China (NSFC) under Grant 61975014, Grant 62035003, and Grant U22A2079, and in part by the Beijing Municipal Science & Technology Commission, Administrative Commission of Zhongguancun Science Park under Grant Z211100004821012. *(Corresponding author: Juan Liu.)*

The authors are with the Beijing Engineering Research Center for Mixed Reality and Advanced Display, MoE Key Lab of Photoelectronic Imaging Technology and System, School of Optics and Photonics, Beijing Institute of Technology, Beijing 100081, China (e-mail: juanliu@bit.edu.cn).

Digital Object Identifier 10.1109/JPHOT.2024.3353786

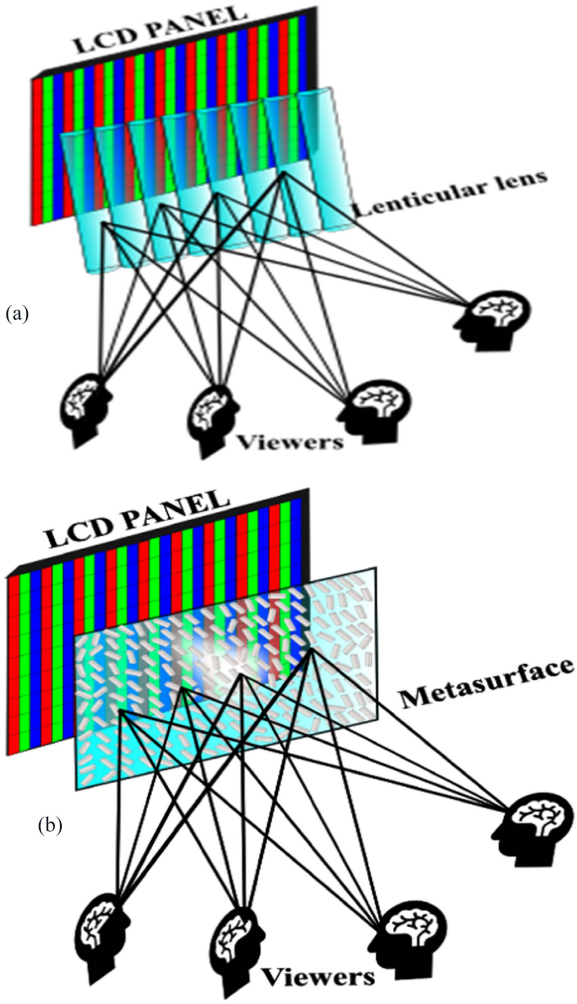

Fig. 1. (a) Schematic diagram of the conventional multiview display by using lenticular lens. (b) Schematic diagram of the proposed multiview display by using metasurface.

and the thickness of the proposed ultrathin metasurface is 2μm. The proposed system reduces the complexity of conventional multiview display systems and also there is an ease to design the system freely by delicate design of nanostructures at the subwavelength scale. The simulation results show that our proposed method can achieve a multiview 3D display with high quality.

II. Principle and Configuration of Ultrathin Metasurface

1) The Wave Transmission of the Designed System for Multi-View Display: Metasurfaces can be designed with precise control over their optical properties, enabling advanced light manipulation and tailored display characteristics. It can provide a wide range of functionalities beyond simple light redirection. This versatility opens up possibilities for more advanced and innovative display designs. Fig. 1(a) and (b) illustrates the schematic of the traditional multiview display systems by using a lenticular lens sheet and the systematic design of the proposed multiview display system by using ultrathin metasurface.

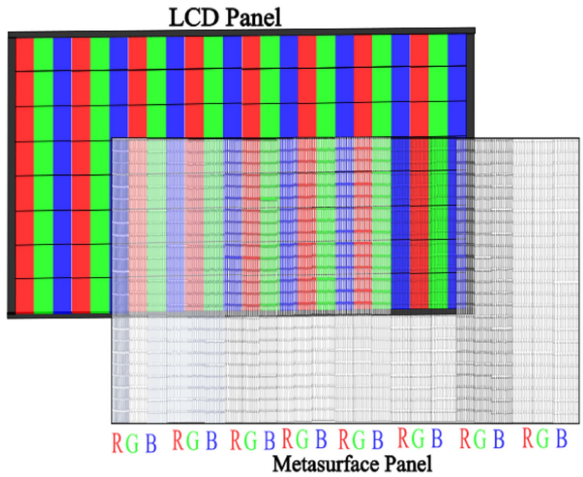

Fig. 2. Schematic diagram of the proposed multiview display by placing metasurface Infront of the LCD panel.

The configuration of the proposed multiview display system is shown in Fig. 2. LCD panel is made up of a number of liquid crystal cells, each of which can individually alter the polarization and transmission of light. The point light source illuminated the display is located behind the LCD panel. The light emanating from each display pixel is directed toward the metasurface. Each pixel in the LCD screen can have its polarization and direction controlled by a metasurface. An array of metasurface is placed in front of LCD panel.

Metasurface array and the subpixel of LCD panel are in one-to-one correspondence according to wavelengths. This array is made up of a grid of tiny nanostructures that manipulate light at the subwavelength scale including amplitude, phase and polarization of light passing through each subpixel. This aspect of the metasurface makes it compact.

By designing the nanostructures carefully, the phase of the incident waves can be manipulated to create desired multiple viewing angles. Moreover, it has different phase profiles across its surface to create multiple views. Every view is associated with a distinct phase profile that transmits the incident light in a specified direction. When multiple viewpoints are combined, a multiview display is produced, allowing viewers to see different images from different perspectives. The views can be arranged arbitrarily within the viewing zone. Individual pixels are intended to provide an image from its corresponding viewpoint. As a result, when switching between views, one can see seamless horizontal motion parallax. Multiple viewing zones or viewpoints allow multiple viewers to perceive different images simultaneously and observe the display from different perspectives; each viewing zone provides a slightly different perspective, enabling a more immersive viewing experience. The specific nanostructures and arrangement of the metasurface elements will depend on the display's desired functionalities and performance requirements. Each nanostructure is associated with a particular panel pixel. Consequently, multiview 3D display has received a lot of interest in becoming a commercially viable autostereoscopic 3D display.

2) Design Methodology for Phase Distribution (LUT): The performance of the polarization-insensitive transparent

metasurface is evaluated in visible regime for red, green, and blue wavelengths ($\lambda = 637$ nm, 532 nm, and 457 nm) by using different period size and varying height of the nanopillars. To interpret the simulation results of the proposed design, the numerical simulations are performed by using the finite-difference time- domain (FDTD) lumerical simulation tool.

The periodic boundary conditions are used in FDTD calculation along x and y direction and perfectly matched layers (PML) are applied in z direction. The unit cell size and the height of the nanopillar are optimized for the desired wavelengths RGB. The metasurfaces are designed by subwavelength rectangular nanopillars of TiO_2. Until now, titanium dioxide TiO_2 which has a refractive index of about 2.6 and is transparent, has been used in the best demonstration of metasurfaces spanning the complete visible regime, resulting in easier phase modulation from 0 to 2π.

To demonstrate simulation results, a linearly x polarized plane EM wave of wavelength 637 nm impinges on the top of the metasurface. The main constituents of metasurface are TiO_2 nanopillar positioned on a glass substrate. The period of the unit cell is $P_x = P_y = 500$ nm and the height of the nanopillar is 600 nm. The exact values of height were obtained by optimization sweeps in FDTD LUMERIC simulations. Simulations are performed to optimize the phase modulation characteristics of the metasurface. A 2D parametric sweep is carried out in the range of 50 to 250 nm by sweeping the length L_x and width L_y of the nanopillar to obtain 0-2π phase coverage which is essential for wavefront modulation. Where L_x & L_y are the lengths of the nanopillars in "x" & "y" directions. 8 nanostructures are selected from the library of parametric sweep with complete phase modulation from 0 to 2π with maximum transmission amplitude as shown in Fig. 3. For a better insight into the phase realization, we calculated the phase of 8 level by using LUT method. LUT store phase information of metasurface units for different phase levels for 0 to 2π phase coverage. By using LUT method we can directly access the corresponding output values for each input pixel values in metasurface design, that eliminates the need for complex calculations.

The phase difference is approximately $\pi/4$ from one neighboring nanostructure to the other. The phase and amplitude of metasurface under the x polarization for the wavelength $\lambda_g = 532$ nm and $\lambda_b = 457$ nm is also calculated as shown in Fig. 3. The height of the nanopillar is 650 nm for λ_g and 400 nm for λ_b with period size 500 nm and 400 nm. 2D parametric sweep is carried out in the range of 80 to 280 nm and 50 to 250 nm for λ_g and λ_b by sweeping the length and width of the nanopillar to obtain 0-2π phase coverage. The actual parametric values of the proposed nanopillars for RGB wavelengths are described in Table I. The look-up table (LUT) method is used to map the metasurface phase for RGB wavelengths with the discrete phase distribution of lenticular lens array to obtain the metasurface array distribution for multiview display.

For an optical system, point spread function (PSF) assess the imaging performance and resolution. It is calculated based on the propagated wavefront in free space. After propagating in free space, the diffuse spot on the image plane is caused by the light waves associated to PSF and the phase information of the metasurface. The PSF of metasurface for RGB wavelengths is shown in Fig. 4.

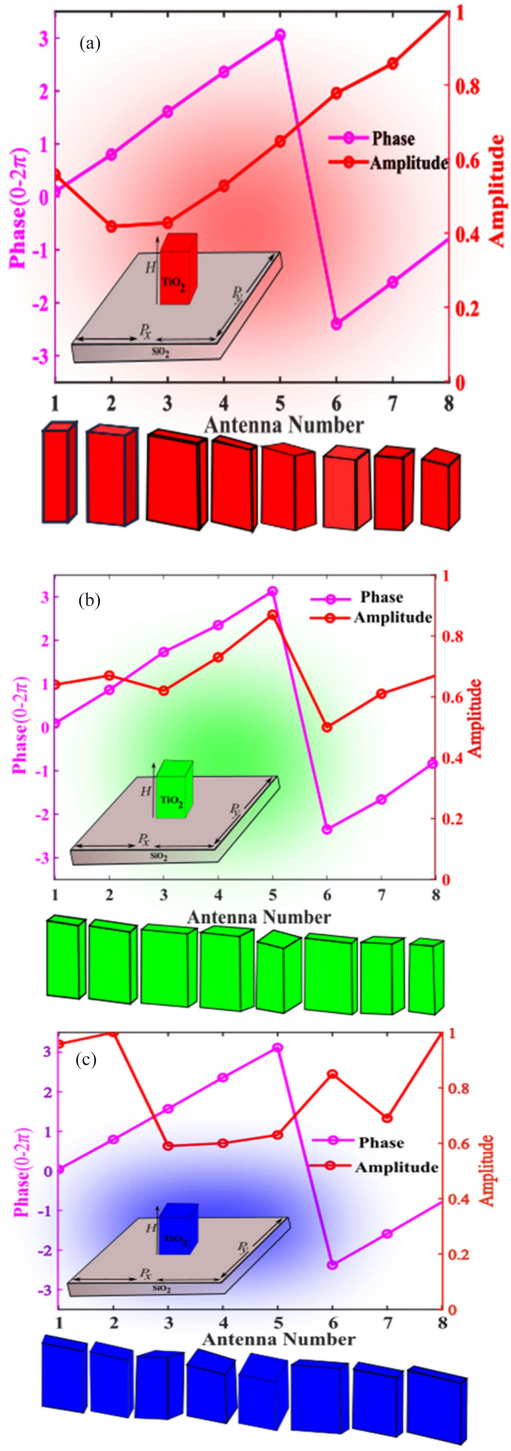

Fig. 3. Numerical simulation results of the 8 selected antennas for (a). Red (b). Green (c) blue wavelengths.

3) Formation of Viewing Zone for Multiview Display: The metasurface in the proposed multiview display system is placed in front of the LCD panel to control the emitted light rays and generate viewpoints in the viewing zone as depicted in Fig. 5.

TABLE I
DEMONSTRATION OF LUT REALIZING THE PHASE DISTRIBUTION, AMPLITUDE AND THE OPTIMIZED PARAMETRIC VALUES OF BASIC NANOPILLARS FOR THE PROPOSED MULTIVIEW DISPLAY SYSTEM

Metasurface design 1 (λ_r=637nm)								
Phase	**0**	$\frac{\pi}{4}$	$\frac{\pi}{2}$	$\frac{3\pi}{4}$	π	$-\frac{3\pi}{4}$	$-\frac{\pi}{2}$	$-\frac{\pi}{4}$
$L_x(nm)$	50	156	250	223	156	210	196	236
$L_y(nm)$	50	63	50	76	210	116	196	196
Metasurface design 2 (λ_g=532nm)								
Phase	**0**	$\frac{\pi}{4}$	$\frac{\pi}{2}$	$\frac{3\pi}{4}$	π	$-\frac{3\pi}{4}$	$-\frac{\pi}{2}$	$-\frac{\pi}{4}$
$L_x(nm)$	146	106	160	146	200	280	106	120
$L_y(nm)$	80	253	80	120	226	80	133	120
Metasurface design 3 (λ_b=457nm)								
Phase	**0**	$\frac{\pi}{4}$	$\frac{\pi}{2}$	$\frac{3\pi}{4}$	π	$-\frac{3\pi}{4}$	$-\frac{\pi}{2}$	$-\frac{\pi}{4}$
$L_x(nm)$	250	223	50	236	236	143	183	250
$L_y(nm)$	63	90	63	143	223	63	50	50

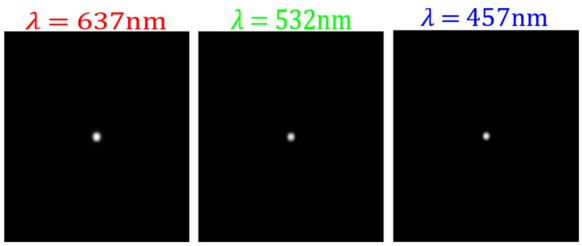

Fig. 4. Simulated PSF of metasurface for RGB wavelengths.

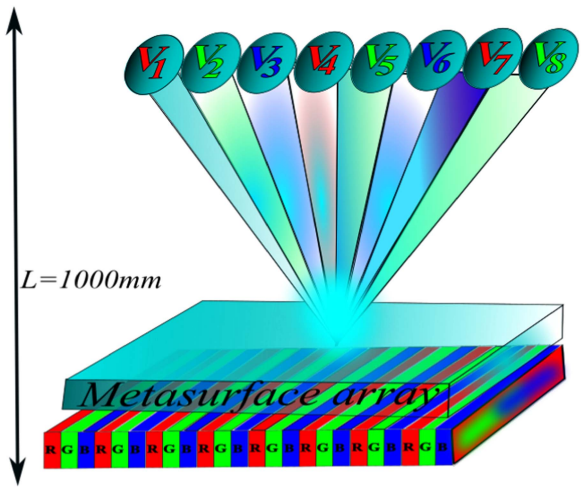

Fig. 5. Demonstration of 8-view display system in a complete display cycle, and the formation of viewing zone.

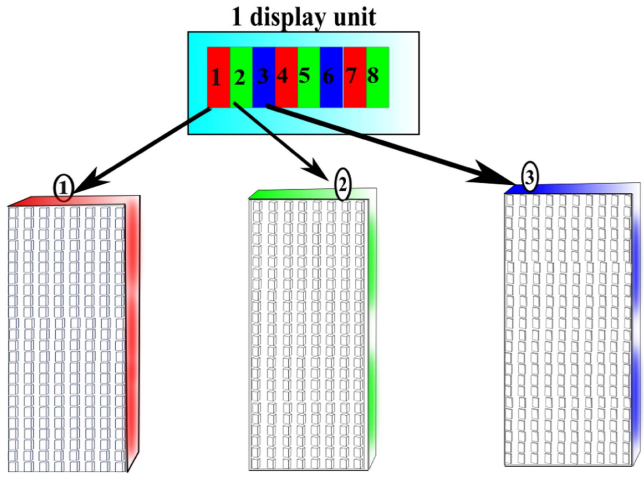

Fig. 6. Subpixels (RGB) to view number mapping.

Light rays carry the light field information loaded on the LCD. The metasurface placed in front of the LCD collects the light rays with light field information and generates the viewpoints at the optimal viewing distance 1000 mm from the LCD screen.

The width of the viewpoint is less than a normal adult's pupillary distance in the viewing zone, so that different images are attained by the right and left eyes. Multiview displays are created by projecting more than 2 viewpoints into each viewer's pupil through the view zone. As, the proposed metasurface covers 8 phase levels for complete wavefront modulation from 0 to 2π, and the viewpoint number equals the number of pixels covered by each display unit.

The precise effects on the viewing zone must rely on the metasurface's design characteristics, capabilities, and overall system configuration. The metasurface selectively controls the phase and amplitude of light rays, redirecting them toward specific viewpoints. The modulated light rays pass through the LCD panel, further controlled by liquid crystal pixels to form the final 3D image. The viewer perceives the image from their viewpoint, as the metasurface redirects the light rays to match their viewing position.

4) Subpixel Mapping: To comprehend the pixel encoding stage, we need to understand that each pixel on the LCD panel corresponds to a specific color. Each pixel on the LCD screen is divided into three subpixels—red, green, and blue—to reproduce color images, and each subpixel's height is three times its width. The intensity of light passing through each subpixel can be controlled, and various colors can be displayed. Fig. 6 illustrates the mapping of the metasurface array with the one display unit that consists of 8 subpixels. The metasurface modulates the red, green, and blue subpixels of an LCD panel. The specific structure of each metasurface unit cell is defined by the viewpoint mapping corresponding to each subpixel. The metasurface panels can be designed to transmit specific wavelengths of light corresponding to the red, green, and blue colors.

We can start from the top-left corner of the LCD panel and assign view number 1 to the first red subpixel, view number

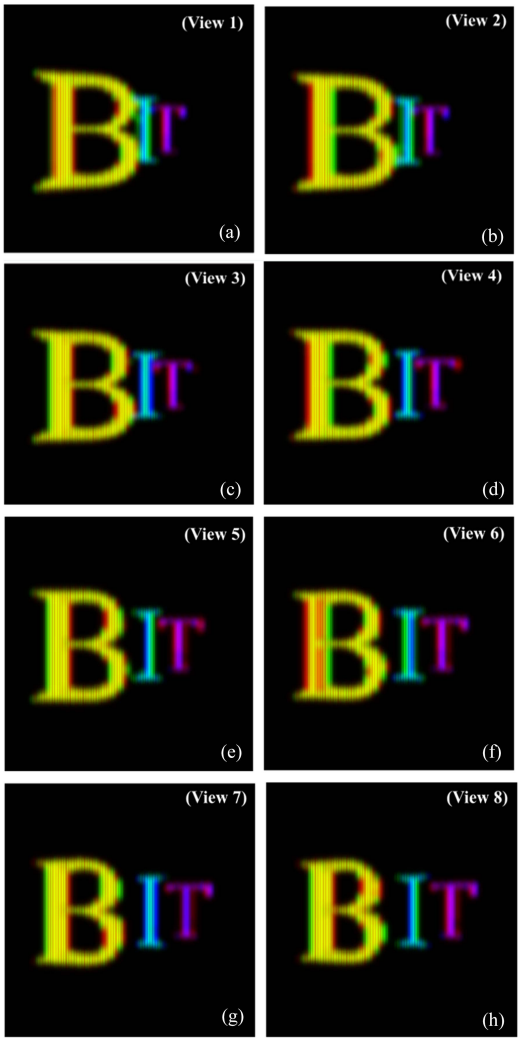

Fig. 7. Display results of an image BIT observed from 8 viewpoints.

2 to the first green subpixel, and view number 3 to the first blue subpixel, then we continue this mapping process for all the subpixels until we reach the bottom-right corner of the LCD panel. By defining this subpixel to view number mapping, we can control the display of colors on the LCD panel by selectively activating the corresponding metasurface panels.

Since the minimum operating unit of the LCD panel is the subpixel, each subpixel contains information of 1 view, as shown in Fig. 6.

The metasurface structure is initially arranged in correspondence with the red subpixel of the LCD panel for a specific viewpoint. So initially for the red subpixel we will arrange the structure 1 for the viewpoint 1 on the metasurface display panel. It means that the metasurface structure is arranged adequately to manipulate the red light to produce the desired image for that viewpoint. Similarly, we can arrange the next structure for the next red subpixel and we continue this procedure until all the structures for the red subpixels arranged properly. The metasurface subwavelength structures are arranged to ensure that the red light is adequately modified and transmitted through the LCD panel for that particular view. So, the metasurface structure is same for one viewpoint but changed for the other. We can control the phase or transmission properties of the light passing through that particular subpixel. This allows for precise control of the propagation of light emitted by the specific subpixel on the LCD panel. It is due to the reason that each subpixel covers different wavelengths but the phase modulation will be same for 1 viewpoint for a single subpixel. The manipulation of phase at the subpixel level is due to the careful metasurface design, mapping, and color calibration processes. The structure must be altered for the other viewpoints, ensuring that the light passing through the display is correctly manipulated to create the desired image. Similarly, we can arrange different metasurface structures effectively and easily on the whole metasurface panel for different wavelengths. However, the metasurface structures needs to be modified for other viewpoints to maintain the intended optical properties. This adjustment can involve changing the arrangement, orientation, or shape of the metasurface structures to ensure that the light passing through the display is manipulated adequately for different views. In green color display by assigning one unit structure to each green subpixel, we can control the phase or transmission properties of the light passing through that particular subpixel and similarly the process continues for the other blue display panel. Depending on the display device's specifications, the synthesized image can be generated through pixel encoding using multi-view images. Every sub-pixel of the synthesized image is derived from various viewpoint images.

III. Results

Virtual cameras are used during the light field pick-up procedure in order to photograph 3D objects in virtual environments. 8 cameras are used, and the number of cameras is equal to the number of viewpoints in the viewing zone. The interval between the viewpoints is 2 mm. The size of the LCD screen is 3.072 $\times$ 3.072 mm and the resolution is 256 $\times$ 256. Fig. 7 illustrates the numerical simulation results of the letter BIT. It is noted from Figs. 7(a) to (h) that the horizontal parallax is observed between the letters B, I and T. When transitioning from one view to another, it gives a pronounced three-dimensional effect. This specifies that the three-dimensional information of the light field is effectively expressed. The simulation results also show that the proposed method by using metasurface in multiview display is feasible and effective and shows the 3D display with high quality. The letters are easily distinguishable**,** ensuring a sharp representation of the characters.

The presented 3D image acquired by the human eyes comprises a series of sub-pixels and is perceived through each sub-unit. The simulation results are achieved by calculating the displayed images for each view. The performance of the proposed method is analyzed by evaluating three quantitative image quality metrics: Root mean square error (RMSE), peak signal-to-noise ratio (PSNR), and structural similarity (SSIM).

The RMSE metric is commonly used to evaluate the accuracy of the reconstructed image. The root mean square error between the original and reconstructed image is defined as,

$$MSE = \frac{1}{N \times N} \sum_{i=1}^{n} \sum_{i=0}^{n} |I(i,j) - k(i,j)|^2 \qquad (1)$$

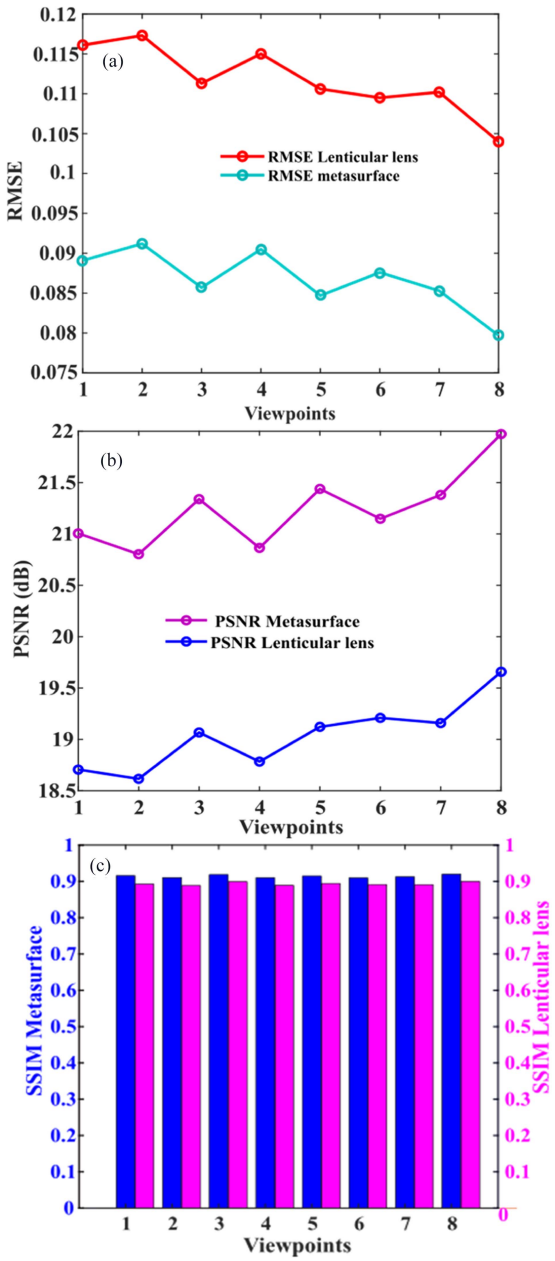

Fig. 8. Comparison curves of performance indicators (a) RMSE, (b) PSNR, (c) SSIM under different perspectives of metasurface based system and lenticular lens based system.

$$\text{RMSE} = \frac{MSE}{\frac{1}{N\times N}\sum_{i=1}^{n}\sum_{i=0}^{n}\left|I\left(i,j\right)-k\left(i,\ j\right)\right|^2} \tag{2}$$

From the above equation, it is assumed that the original image and the reconstructed image is represented by *I* and *K, I (i, j)* mean the pixel value in the row and column in the original distribution. In contrast, *K (i, j)* represents the value of the corresponding pixel in the reconstructed image [39]. The proposed multiview display system reconstructs an image from multiple viewpoints to produce a more enticing and realistic viewing experience. Fig. 8(a) represents the RMSE value of metasurface based system and lenticular lens-based system. The RMSE value in the graph shows a measure of the overall difference between the original and the reconstructed image. A lower value of RMSE in the graph for the corresponding viewpoint indicates a closer match between the original and reconstructed image. It implies higher consistency and quality in the reconstructed image, allows for a more comprehensive evaluation of the display system's performance, and helps to identify the discrepancies and potential issues in the reconstructed images. So, it is clear from Fig. 8(a) that the proposed metasurface based display system is good in performance as compared to lenticular lens based conventional systems.

A full-reference criterion for evaluating image quality is PSNR. The ratio of the maximal signal power to the noise power is PSNR. The higher the PSNR value is, the less distorted the reconstructed images are. The PSNR is defined as follows [39].

$$\text{PSNR} = 10 \times \log_{10}\left(\frac{\text{Max}\left(I\right)}{MSE}\right) \tag{3}$$

Fig. 8(b) shows the PSNR of the displayed images from 8 different viewpoints. The points on the graph represent the PSNR values of the eight different viewpoints in the multiview display. Each point in the graph corresponds to a specific viewpoint. The higher the PSNR value in the graph represents, the less distorted the reconstructed images. This means that the image quality is preserved better for those viewpoints with less distortion, resulting in a more realistic and accurate representation. The significant variations in the graph with different perspectives suggest that the distortion in the reconstructed image may vary across different viewpoints. It is clear from the Fig. 8(b) that the PSNR of our proposed system by using metasurface is higher as compared to lenticular lens-based system that indicates the performance of our proposed system is quite better than the conventional system where lenticular lens is used.

Through the use of the mean value, square deviation, and covariance of the original image and recovered image, the structure similarity index (SSIM) is computed [39]. It is based on an image distortion model that considers three factors: luminance distortion, loss of correlation, and contrast distortion, and it determines the similarity between two images.

The SSIM index, which is based on a distortion-free image or an uncompressed image as the reference, is calculated for 8 viewpoints in order to access these created images seen from 8 viewpoints. The SSIM values for 8 viewpoints are displayed in Fig. 8(c). This illustrates that the SSIM values of our proposed multiview display by using metasurface for the first time are quite adequate as compared to conventional system where lenticular lens are used. The bar graph represents the SSIM values of the 8 different viewpoints in the multiview display system. Each bar in the graph corresponds to a specific viewpoint. The height of the bar indicates the SSIM value, with higher bars representing higher similarity between the displayed content and the reference image. Viewpoints with higher bars show a higher similarity between the displayed content and the reference image. This means that the image quality is preserved better from those viewpoints result in a more realistic and accurate representation. If there are significant variations in the bar heights, the image quality may vary across different perspectives. The proposed multiview display facilitates the quality of 3D images.

IV. Conclusion

This paper presents a multiview 3D display by using an ultrathin metasurface that modulates the phase and amplitude of light waves. This opens new opportunities to solve the formidable problems in conventional multiview displays, such as system complexity and freedom to design. The subpixels of metasurface for RGB wavelengths having one to one correspondence with the LCD subpixels. The phase of metasurface is mapped with the phase of lenticular lens by using LUT method. 8 views are implemented in numerical simulation and the thickness of metasurface layer is 2 μm, which leads to a high-quality, ultrathin multiview 3D display. The development of the proposed multiview 3D display with ultrathin metasurface would pave the way toward realizing next-generation compact displays. It also demonstrates the ultimate goal of future 3D TVs and mobile electronics. Moreover, it can also be used for medical and educational applications in the near future.

Acknowledgment

The authors declare no conflicts of interest.

References

[1] K. Suzuki, Y. Fukano, and H. Oku, "1000-volume/s high-speed volumetric display for high-speed HMD," *Opt. Exp.*, vol. 28, no. 20, pp. 29455–29468, 2020.

[2] D. Smalley et al., "A photophoretic-trap volumetric display," *Nature*, vol. 553, no. 7689, pp. 486–490, 2018.

[3] Y. Jo, S. Lee, D. Yoo, S. Choi, D. Kim, and B. Lee, "Tomographic projector: Large scale volumetric display with uniform viewing experiences," *Assoc. Comput. Machinery Trans. Graph.*, vol. 38, no. 6, pp. 1–13, 2019.

[4] M.-H. Choi, K.-S. Shin, J. Jang, W. Han, and J.-H. Park, "Waveguide-type Maxwellian near-eye display using a pin-mirror holographic optical element array," *Opt. Lett.*, vol. 47, no. 2, pp. 405–408, 2022.

[5] D. Pi, J. Liu, and Y. Wang, "Review of computer-generated hologram algorithms for color dynamic holographic three-dimensional display," *Light: Sci. Appl.*, vol. 11, no. 1, 2022, Art. no. 231.

[6] X. Wang and H. Hua, "Design of a digitally switchable multifocal microlens array for integral imaging systems," *Opt. Exp.*, vol. 29, no. 21, pp. 33771–33784, 2021.

[7] R. Zhou et al., "Depth of field expansion method for integral imaging based on diffractive optical element and CNN," *Opt. Exp.*, vol. 31, no. 23, pp. 38146–38164, 2023.

[8] Y. Xing et al., "Integral imaging-based tabletop light field 3D display with large viewing angle," *Opto-Electron. Adv.*, vol. 6, no. 6,2023, Art. no. 220178.

[9] P. Wang et al., "Demonstration of a low-crosstalk super multi-view light field display with natural depth cues and smooth motion parallax," *Opt. Exp.*, vol. 27, no. 23, pp. 34442–34453, 2019.

[10] K. Akşit, A. H. G. Niaki, E. Ulusoy, and H. Urey, "Super stereoscopy technique for comfortable and realistic 3D displays," *Opt. Lett.*, vol. 39, no. 24, pp. 6903–6906, 2014.

[11] Y. Watanabe and H. Kakeya, "Time-division and color multiplexing light-field display using liquid-crystal display panels to induce focal accommodation," *Appl. Opt.*, vol. 60, no. 7, pp. 1966–1972, 2021.

[12] L. Liu, J. Cai, Z. Pang, and D. Teng, "Super multi-view near-eye 3D display with enlarged field of view," *Opt. Eng.*, vol. 60, no. 8, p. 085103, 2021.

[13] L. Yang et al., "A crosstalk-suppressed dense multi-view light-field display based on real-time light-field pickup and reconstruction," *Opt. Exp.*, vol. 26, no. 26, pp. 34412–34427, 2018.

[14] F. Zilly, M. Müller, and P. Kauff, "Generic content creation for 3D displays," in *3D-TV in System With Depth-Image-Based Rendering: Architectures, Techniques and Challenges*. Berlin, Germany: Springer, 2013, pp. 39–68.

[15] X. Xia, X. Zhang, L. Zhang, P. Surman, and Y. Zheng, "Time-multiplexed multi-view three-dimensional display with projector array and steering screen," *Opt. Exp.*, vol. 26, no. 12, pp. 15528–15538, 2018.

[16] M. Ahmad, "Wideband reflective half-and quarter-wave plate metasurface based on multi-plasmon resonances," *Opt. Continuum*, vol. 2, no. 5, pp. 1242–1255, 2023.

[17] U. U. R. Qureshi, B. Hu, M. I. Khan, and M. Ahmad, "Multifunctional active terahertz metasurface with electromagnetically induced transparency, perfect absorption, and circular dichroism," *Opt. Commun.*, vol. 550, 2024, Art. no. 129989.

[18] X. Luo, "Subwavelength artificial structures: Opening a new era for engineering optics," *Adv. Mater.*, vol. 31, no. 4, 2019, Art. no. 1804680.

[19] U. U. R. Qureshi, B. Hu, S. Basir, M. Ahmad, A. Jalal, and M. I. Khan, "Design and experimental realization of multifunctional anisotropic metasurface for efficient polarization manipulation in microwave frequencies," *Physica Scripta*, vol. 99, 2023, Art. no. 015512.

[20] N. Yu et al., "Light propagation with phase discontinuities: Generalized laws of reflection and refraction," *Science*, vol. 334, no. 6054, pp. 333–337, 2011.

[21] N. Meinzer, W. L. Barnes, and I. R. Hooper, "Plasmonic meta-atoms and metasurfaces," *Nature Photon.*, vol. 8, no. 12, pp. 889–898, 2014.

[22] N. Yu and F. Capasso, "Flat optics with designer metasurfaces," *Nature Mater.*, vol. 13, no. 2, pp. 139–150, 2014.

[23] S. Zhu et al., "Liquid crystal integrated metadevice for reconfigurable hologram displays and optical encryption," *Opt. Exp.*, vol. 29, no. 6, pp. 9553–9564, 2021.

[24] P. Genevet, F. Capasso, F. Aieta, M. Khorasaninejad, and R. Devlin, "Recent advances in planar optics: From plasmonic to dielectric metasurfaces," *Optica*, vol. 4, no. 1, pp. 139–152, 2017.

[25] A. I. Kuznetsov, A. E. Miroshnichenko, M. L. Brongersma, Y. S. Kivshar, and B. Luk'yanchuk, "Optically resonant dielectric nanostructures," *Science*, vol. 354, no. 6314, 2016, Art. no. aag2472.

[26] X. Ni, N. K. Emani, A. V. Kildishev, A. Boltasseva, and V. M. Shalaev, "Broadband light bending with plasmonic nanoantennas," *Science*, vol. 335, no. 6067, p. 427, 2012.

[27] D. Wen, J. J. Cadusch, J. Meng, and K. B. Crozier, "Light field on a chip: Metasurface-based multicolor holograms," *Adv. Photon.*, vol. 3, no. 2, 2021, Art. no. 024001.

[28] J. Yang et al., "Achromatic flat focusing lens based on dispersion engineering of spoof surface plasmon polaritons," *Appl. Phys. Lett.*, vol. 110, no. 20, 2017, Art. no. 203507.

[29] U. U. R. Qureshi, M. I. Khan, and B. Hu, "Realizing efficient THz circular dichroism using ultra-thin chiral metasurface," *Physica Scripta*, vol. 98, 2023, Art. no. 075513.

[30] U. U. R. Qureshi, B. Hu, M. Ahmad, and A. Jalal, "Graphene-based triple-band tunable metasurface with strong circular dichroism for Hz communication," *IEEE Photon. Technol. Lett.*, vol. 35, no. 24, pp. 1375–1378, Dec. 2023.

[31] L. Zhang, J. Guo, and T. Ding, "Ultrathin dual-mode vortex beam generator based on anisotropic coding metasurface," *Sci. Rep.*, vol. 11, no. 1, 2021, Art. no. 5766.

[32] R. A. Aoni et al., "High-efficiency visible light manipulation using dielectric metasurfaces," *Sci. Rep.*, vol. 9, no. 1, 2019, Art. no. 6510.

[33] A. U. R. Khalid, J. Liu, Y. Han, N. Ullah, S. Jia, and Y. Wang, "Multipurpose thermoresponsive hydrogel: A platform for dynamic holographic display," *Opt. Lett.*, vol. 45, no. 2, pp. 479–482, 2020.

[34] C. Jin et al., "Dielectric metasurfaces for distance measurements and three-dimensional imaging," *Adv. Photon.*, vol. 1, no. 3, 2019, Art. no. 036001.

[35] Y. Ni, S. Chen, Y. Wang, Q. Tan, S. Xiao, and Y. Yang, "Metasurface for structured light projection over 120 field of view," *Nano Lett.*, vol. 20, no. 9, pp. 6719–6724, 2020.

[36] G.-Y. Lee, J. Sung, and B. Lee, "Metasurface optics for imaging applications," *Mater. Res. Soc. Bull.*, vol. 45, no. 3, pp. 202–209, 2020.

[37] Y. Zhang et al., "Crosstalk-free achromatic full Stokes imaging polarimetry metasurface enabled by polarization-dependent phase optimization," *Opto-Electron. Adv.*, vol. 5, no. 11, 2022, Art. no. 220058.

[38] G. Kim et al., "Metasurface-driven full-space structured light for three-dimensional imaging," *Nature Commun.*, vol. 13, no. 1, 2022, Art. no. 5920.

[39] X. Yu, R. I. Stantchev, F. Yang, and E. Pickwell-MacPherson, "Super sub-nyquist single-pixel imaging by total variation ascending ordering of the hadamard basis," *Sci. Rep.*, vol. 10, no. 1, 2020, Art. no. 9338.